Evolution of a confluent gut epithelium under on-chip cyclic stretching

Lauriane Gérémie, Efe Ilker, Moencopi Bernheim-Dennery, Charles Cavaniol, Jean-Louis Viovy, Danijela Matic Vignjevic, Jean-François Joanny, Stéphanie Descroix

Evolution of a confluent gut epithelium under on-chip cyclic stretching

Lauriane Gérémie,[1,2,*] Efe Ilker,[1,2,3,*,†] Moencopi Bernheim-Dennery,[1,2] Charles Cavaniol,[1,2] Jean-Louis Viovy,[1,2] Danijela Matic Vignjevic,[1,4] Jean-François Joanny,[1,2,5,‡] and Stéphanie Descroix[1,2,§]

[1]*Laboratoire Physico-Chimie Curie, Institut Curie, PSL Research University, CNRS UMR 168, Paris, France*
[2]*Sorbonne Universités, UPMC Univ. Paris 06, Paris, France*
[3]*Max Planck Institute for the Physics of Complex Systems, 01187 Dresden, Germany*
[4]*Institut Curie, Cell Migration and Invasion, PSL Research University, CNRS UMR 144, Paris, France*
[5]*Collége de France, 11 place Marcelin Berthelot, 75005 Paris, France*

(Received 19 October 2021; accepted 7 March 2022; published 11 April 2022)

The progress of food in the gastrointestinal (GI) tract is driven by a peristaltic motion generated by the muscle belt surrounding the GI tract. In turn, the response of the intestinal epithelial cells to the peristaltic stresses affects the dynamics of the epithelial structure. In this work, we study the effect of cyclic stretching (0.125 Hz, 10% strain) on the spatial organization of the intestinal epithelium using intestinal cells deposited on a flat elastomeric substrate to mimic the peristaltic motion *in vitro*. A confluent monolayer of Caco-2 cells is grown on a PDMS chip to probe the morphological and orientational response of the tissue to cyclic stretching. The PDMS chips are either covalently or noncovalently coated with laminin to recapitulate the basement membrane. We observe a significant orientational response where the cells rearrange their long axes perpendicular to the stretching direction for both coating conditions. The experiment is modeled by a vertex model where the cells store elastic energy with varying strain and effectively have a rotational diffusive motion of their long axes through rearrangements of their shapes. The model also predicts a transition between the perpendicular orientation and the orientation at an oblique angle determined by the level of the cell elastic anisotropy. It provides a general framework to study cell response and relaxation dynamics under cyclic stretching across different cell types. We also discuss potential relevance of peristalsis in determining planar cell polarity in three-dimensional architectures.

DOI: 10.1103/PhysRevResearch.4.023032

I. INTRODUCTION

The small intestine is a major organ of the human body, the place of nutrient absorption and a barrier against external entities. These functions are in part achieved by the epithelial monolayer that faces the intestinal lumen. The epithelium is attached to the basement membrane (BM) composed of laminin and collagen IV. The BM offers structural support for the epithelium and separates it from the stroma. The stroma consists of cellular components such as fibroblasts, immune and endothelial cells, and a supporting network of extracellular matrix (ECM).

The intestine is a complex organ with unique three-dimensional (3D) structure and dynamics. It possesses an intricate topography composed of fingerlike protrusions, called villi, and crypts that descend into the stroma. These different regions are correlated with a well-defined patterning of various cell types: the intestinal stem cells are confined at the bottom of the crypts, whereas most of the differentiated cells migrate actively from the crypts to the tip of the villi where they are extruded from the monolayer [1]. In addition to being regulated by a wide range of topographical cues, the small intestine epithelium experiences various mechanical forces in both physiological and pathophysiological states [2]. In particular, intestinal epithelial cells are exposed to shear stress, cyclic deformation, and strain associated with villi motility. These forces affect cell properties, such as proliferation or adhesion, and tissue properties, such as the intestinal barrier function [3–5]. A significant source of mechanical stress is the peristaltic motion that arises from two layers of smooth muscles, the outer layer oriented longitudinally and the inner oriented circumferentially [6]. Their contractions take place at different frequencies and amplitudes depending on food uptake and are highly coordinated to act as propulsive forces and to mix the lumen content [7].

Over the past decade, there have been remarkable efforts to recapitulate *in vitro* complexity of gut anatomy. The most commonly used model is organoids generated from mouse intestine. They spontaneously form protrusions resembling crypts and exhibit normal cell differentiation and localization of intestinal stem cells. However, the lack of villus

*These authors contributed equally to this work.
†ilker@pks.mpg.de
‡jean-francois.joanny@college-de-france.fr
§stephanie.descroix@curie.fr

domain and the organoids' closed structure are clear limitations [8,9]. Organ-on-chip technology is an appealing alternative to organoids as it aims at recapitulating multicellular architectures, physical, biochemical, and geometrical features of a specific organ on a microfluidic chip [10,11]. Two main approaches are undertaken to develop a relevant gut-on-chip model. The first approach is to build a 3D scaffold that replicates the villi/crypt structure on which cells are seeded [12–15]. On such 3D scaffolds, cell segregation along the crypt-villus axis is achieved either by implementing growth factor gradients [16] or with the addition of stromal cells [17]. The second approach relies on applying external forces on cells to mimic the intestinal dynamics, which have been studied in 2D systems only [18–21]. In most models, cells are grown on deformable membranes, and cells are subjected to both stretch and shear stresses [3,22]. The relative importance of these two mechanical stresses *in vivo* regarding their effect on intestinal cells is not elucidated yet. However, *in vitro* 2D studies allow to discriminate between the two stresses. They have shown that the application of physiological fluidic flow across the apical surface of the epithelium accelerates cell polarization while cyclic stretching does not [23]. They also showed by measuring enzymatic activity that the combination of shear stress and cyclic stretching improves cell differentiation, and more recently *in vitro* studies have demonstrated that cyclic stretching is required to mimic the *in vivo* parasite invasion of the gut epithelium [22]. After about 100 h of stretching, cells spontaneously form folds resembling villi, and epithelial barrier function improves compared with no strain conditions [23]. The transcriptomic study showed that cells grown on those chips resemble the *in vivo* conditions more closely than organoids [24].

These recent papers have highlighted how mechanical forces applied to cells are instrumental in developing a relevant *in vitro* microphysiological gut model. While most studies address how cyclic stretching that mimics peristaltic motion impacts intestinal cell proliferation or differentiation, it remains unclear how the tissue organization is affected by these forces. Here we address this question and focus on the effect of peristaltic motion in the organization of intestinal epithelium. To this aim, we developed a novel stretching device compatible with microfluidic chips that recapitulate both the BM and the intestinal epithelium. We study two coating conditions of the BM; laminin is either covalently or noncovalently coated on the PDMS chip. Next, we apply cyclic stretching on the chip where the intestinal epithelium is subject to a 10% strain at 0.125 Hz mimicking the *in vivo* peristaltic motion [21]. We next characterize the monolayer response to cyclic stretching in terms of cell spatial organization and morphology within the tissue for a wide range of stretching times to explore the kinetics of the tissue response. The most significant response of the tissue appears in the cell reorientation: a fraction of the cells orients their long axis perpendicular to the stretching direction. In the case of isolated and highly contractile needlelike cells, earlier theoretical studies explored the anisotropic response minimizing an elastic energy [25] or the active response required to maintain tensional homeostasis [26–28]. In our description of tissues, we model this behavior using a vertex model that includes both aspects and we combine it with an overdamped dynamics of the cell reorientation. We identify the effects of cell anisotropy and activity in determining the cell orientation under peristaltic stimuli. We propose a general theory of the reorientational response of cell populations in which size-dependent interactions and long-range correlations are negligible.

II. RESULTS

A. Cell monolayer culture and stretching device

To assess the influence of stretching and cyclic stretching on the intestinal epithelium, we developed a customized stretching device along with dedicated microfluidic chip fabrication [Fig. 1(a)]. The stretching device is compatible with conventional cell culture conditions and can accommodate three chips in parallel, and its mechanical strain and frequency can be tuned at will. In comparison, the most commonly used model of dynamic gut-on-chip is based on the use of a central cell culture chamber separated by a thin porous membrane flanked with two vacuum lateral channels that are used to perform cyclic stretching [29]. Those devices have shown their potential for different cell types [23,30] as they allow an efficient strain application. However, they require complex microfabrication and microfluidic-based fluid handling. Here we develop an original microfabrication approach to design open chips similar to a conventional cell culture dish compatible with stretching. The bottom of the chip where the cells are grown could be either flat as in the current work or 3D structured. These chips are made of polydimethylsiloxane (PDMS), a common cytocompatible elastomer used here as cell culture substrate [Fig. 1(b)]. The PDMS prepolymer and curing agent ratio is set to 10:1 (w/w) with a Young modulus around 1.63 MPa [31]. Stretching creates a biaxial strain at the center of the chip with a longitudinal elongational strain u_{xx}^{lab} and a transverse contractile strain $u_{yy}^{\mathrm{lab}} = -\nu u_{xx}^{\mathrm{lab}}$ where the measured Poisson ratio of the substrate is $\nu = 0.4$. We quantify the cells' response to cyclic stretching only at the central part of the chip where the deformation can be considered homogeneous [Fig. 1(c)].

To reproduce the composition of the intestinal mucosa, we first recapitulated the intestinal BM by coating the chips with laminin [Fig. 1(b)], the predominant BM glycoprotein [32]. The cell response to ECM deformation is mediated by focal adhesions (FAs) that link the cell to the substrate. FA protein, paxillin, is activated during the cyclic deformation of intestinal cells [33]. To model *in vitro* the cell-BM interactions, PDMS could be coated with adsorbed BM proteins such as laminin or collagen IV. More recently, Wipff *et al.* proposed an original approach to covalently coat ECM proteins to stretchable PDMS membrane, which circumvents some limitations of noncovalent coating in particular its poor stability [34].

Here we tested both coating procedures to assess how the coating conditions affect the epithelium response to cyclic stretching, assuming that a more stable attachment of laminin to the surface could improve cell adhesion. More precisely, the PDMS coating is performed either covalently, through PDMS silanization coupled by glutaraldehyde cross-linking (as described in [34]), or noncovalently, through physisorption after PDMS activation by plasma treatment. To recapitulate

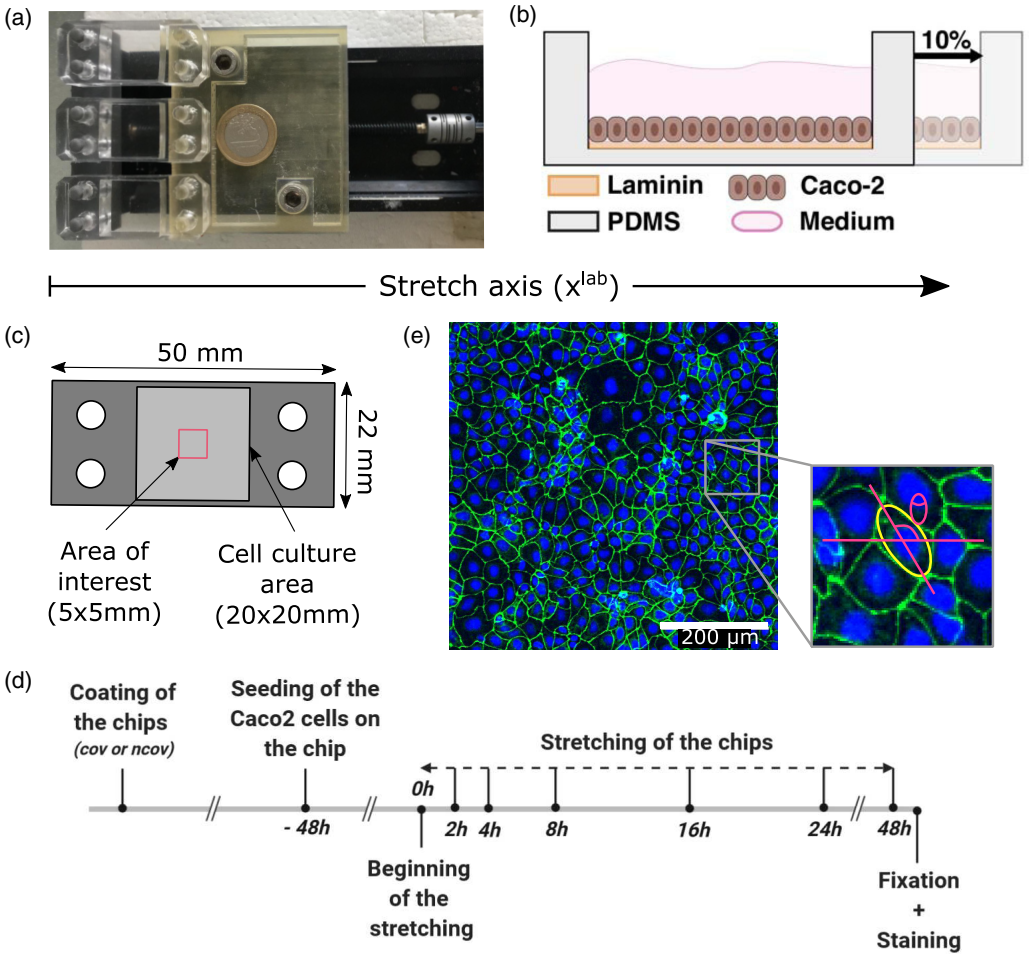

FIG. 1. (a) Picture of the homemade stretching device allowing the stretching of three chips in parallel. (b) Schematic cross-section of the chip representing the BM, the cells as well as the stretching deformation. (c) Schematics of the chip representing the area of interest where imaging is performed. (d) Time line of the experimental workflow from the chip coating to cell staining. (e) Picture of the confluent Caco-2 monolayer after 24 h of stretching with a laminin covalent coating using a 10× confocal microscope. The tight junctions are stained using ZO1 antibody (in green) and nucleus staining is performed using Hoecht (in blue). The insert shows the ellipse fit by ImageJ to estimate the cell long and short axis as well as cell orientation angle (θ) with respect to the stretching direction.

the human intestinal epithelium, we grew the human colon carcinoma cell line (Caco-2) 48 h on those chips so that they reached confluence before stretching [Fig. 1(d)]. The Caco-2 cell line has been selected because it generates a tight epithelial monolayer and it is a common model to study the intestinal epithelium [3,15,35,36].

B. Effect of uniaxial cyclic stretching on epithelium morphology

To asses how stretching affects epithelial cells, we subjected the epithelial intestinal monolayer to a cyclic stretching, mimicking the intestinal peristalsis *in vivo*. We implemented a sinusoidal strain $u_{xx}^{\text{lab}}(t) = u(t) = \frac{1}{2}u_0(1 - \cos(\omega t))$ and $u_{yy}^{\text{lab}}(t) = -\nu u(t)$ with angular frequency $\omega = 0.125\,\text{Hz} \cdot 2\pi$ and magnitude $u_0 = 0.1$ imposed during a period ranging from 2 to 48 h to measure the kinetics of the intestinal epithelium response. As a control, we used similar chips seeded with the Caco-2 cells but left deformation-free during the experiment.

In order to probe morphological changes in the tissue, we stained tight junctions using ZO1 (Zonula occludens-1). In both conditions, Caco-2 cells formed a tight monolayer with prominent tight junctions between cells. This epithelial monolayer was tightly packed with columnar cells with a hexagonal-like shape at their apical side characteristic of *in vivo* intestinal epithelium [Fig. 1(e)]. We analyzed cell circularity, perimeter, and area using Tissue Analyzer plugins in Fiji software. Cells were fitted by an ellipse from which we measured their long and short axes to infer their aspect ratio and the orientation of their long axis with respect to the stretch direction.

We first examine if the laminin coating strategy affects intestinal cell morphology in the absence of stretching. Indeed, it has been shown that laminin surface density can be increased by covalent coating [37] compared with noncovalent coating, which could consequently affect cell spreading. We observed that the cell area was similar on covalently and noncovalently coated PDMS even after 24 h of culture. This result suggests that the different coating strategies do not affect cell spreading. We next examined cell response to cyclic stretching. We found that even after a long stretching period, stretching does not affect the general morphology of

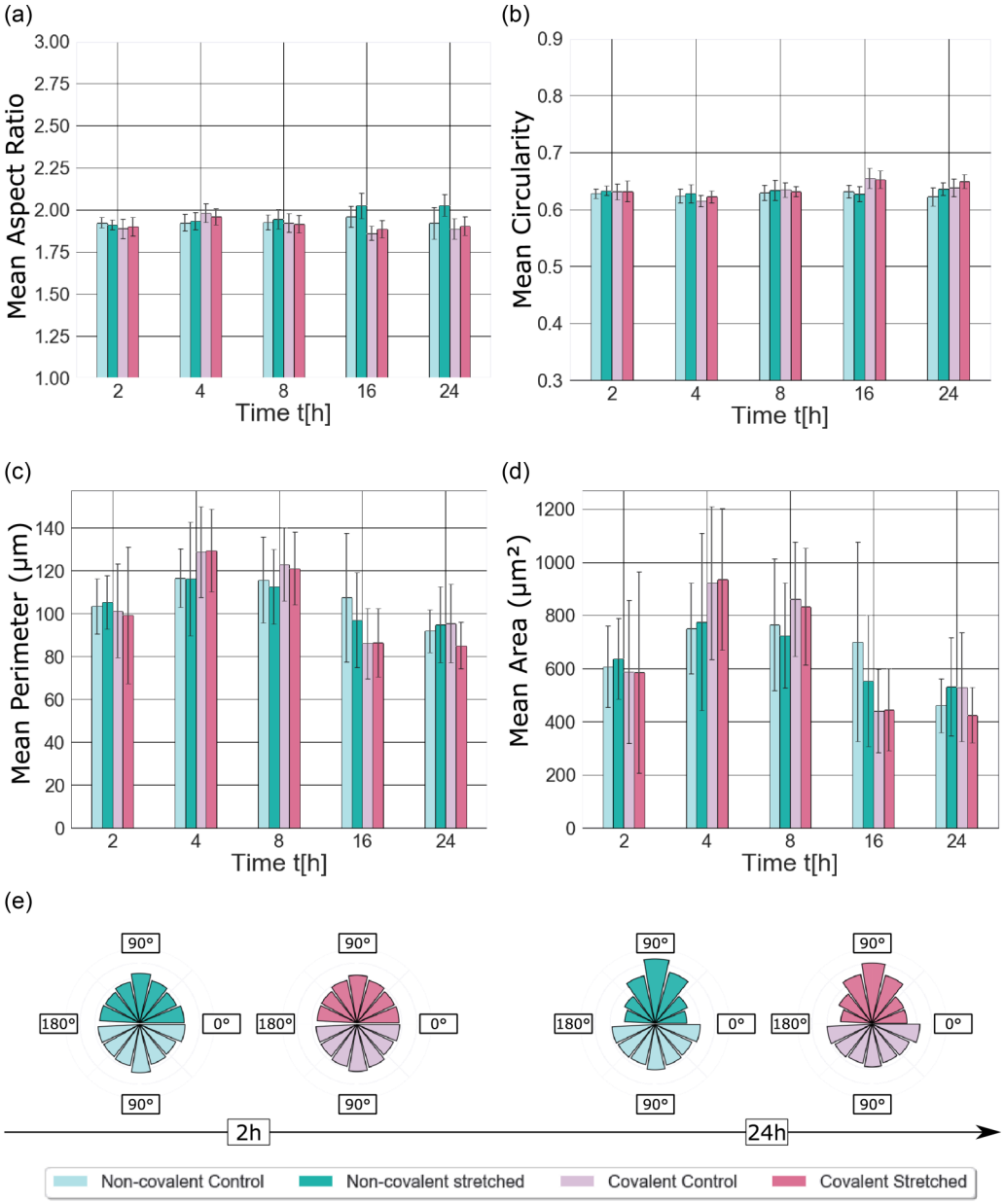

FIG. 2. Variation of shape parameters of epithelial cells for different analysis times t under cyclic stretching with $u_{xx}^{\text{lab}}(t) = u(t) = \frac{1}{2}u_0(1 - \cos(\omega t))$ with $\omega = 0.125\,\text{Hz} \cdot 2\pi$ and magnitude $u_0 = 0.1$. The mean aspect ratio (a), circularity (b), perimeter (c), and area (d) are plotted as a function of time for covalent and noncovalent coating and stretched and control conditions. These data have been collected from 15 images (5 images per chip) which correspond approximately to 20,000 cells analyzed per condition. We calculated the mean parameter per image, and the error bars are obtained by the standard deviation between images of the same condition. All cell shape parameters remain constant over time and do not vary as functions of the stretching conditions. Panel (e) shows the angular distribution of cell orientations after 2 h (left) and 24 h (right) of stretching for covalent and noncovalent coating and stretched and control conditions. The percentage of cells perpendicular to the stretching direction increases with stretching time.

the intestinal cells except for long axis orientation which is sensitive to the mechanical stimulus. In particular, the mean area, perimeter, aspect ratio, or circularity of cells are similar between stretched and control conditions, as well as between covalently and noncovalently bound laminin [Figs. 2(a)–2(d)]. Similarly, we did not observe any change of the monolayer height between different conditions (data not shown).

Nevertheless, after 48 h of cyclic stretching, patches of cells start to detach from the cell substrate that is noncovalently coated with laminin, while no detachment is observed with covalently coated laminin. Similar observations have been reported for human aortic smooth muscle cells grown on submillimeter hemichannels made of glass which is either covalently or noncovalently coated with collagen I [38]. Higher substrate curvature or cell contractility results in increased cell detachment, which is likely due to an imbalance between cell-generated forces and the strength of cell-cell and cell-substrate adhesions. As our substrates are flat, cell detachment is likely due to an imbalance between stretch-induced cell forces and cell-substrate adhesion strength. These results are in good

agreement with the lower stability of the noncovalent coating reported elsewhere [37].

Altogether, our results show that the cell shape parameters are insensitive to a cyclic stretch mimicking *in vivo* peristalsis regardless of the laminin coating conditions and remain constant over time. However, we noticed an anisotropic response of the cells measured by the orientation angle of their long axis, which we examine next in detail.

C. Epithelial cells reorient perpendicular to principal strain direction under cyclic stretching

During periodic stretching, the cells are under varying strain such that there is no unique rest position on the stretching path from the reference state (RS; nonstretched, $u_{xx}^{\text{lab}} = 0$) to the stretched state. Thus the cells continuously feel the varying mechanical stimuli and store elastic energy. Our results show that, in these conditions, a significant fraction of cells orient perpendicular to the stretching direction. As illustrated in Fig. 2(e), after 24 h of cyclic stretching, ∼20% of the total cell population orient between 80 and 100° to the stretching direction.

Previous works report a passive response to a finite nonvarying stretch in which cells tend to orient parallel to the stretching direction [39,40]. We also performed static stretch experiments that are detailed in Appendix C and observed a similar passive response. However, if the chip remains under constant strain $u(t) = u_0$ during several hours, we observe a dissipative relaxation of cell orientation without any stored elastic energy, showing the reversibility of orientational behavior. Starting from an orientation that was parallel with the stretching direction, the ensemble of cells recovers orientational isotropy with an orientational relaxation time $\tau_{\text{rel}} \sim 5 - 7\,\text{h}$. In contrast, during cyclic stretching, the cells can store elastic energy, as discussed in the following.

To model the orientational dynamics under cyclic stretching, we make the following assumptions: (i) Cells deform together with the substrate and hence passively follow the stretch direction at short times ($t \sim \tau_{\text{str}}$) where $\tau_{\text{str}} = 2\pi/\omega$ is the period of stretching. (ii) At long time scales ($t \gg \tau_{\text{str}}$), the long axes of cells undergo a rotational diffusion. In the absence of strain, this leads to an isotropic distribution of orientations. As we exert cyclic stretching, the cells are subject to an angle-dependent potential as detailed below.

We write the total elastic energy stored in the tissue under varying strain using a vertex model. For a tissue containing N confluent cells, the total mechanical energy is given by $E_{\text{tot}} = E_{\text{tot}}(\{\mathbf{r}_i\})$ [41–43],

$$E_{\text{tot}} = \sum_{i=1}^{N} K_A(A_i - A_0)^2 + \gamma_P P_i + K_P P_i^2. \tag{1}$$

Each cell i at position $\mathbf{r}_i$ has a preferred area $A_{i,0} = A_0$ that we consider identical for all cells. If a cell has an area A_i different from A_0, there is an energy cost with a positive modulus K_A. The second term is a line energy proportional to the cell perimeter P_i. At linear order, the line tension is $\gamma_P P_i$. This line tension includes contributions both from cell-cell adhesion and individual cell cortical tension. Because of the cell activity, the line tension depends on the cell perimeter and this leads to a correction $K_P P_i^2$. For stability reasons, the perimeter modulus K_P is also positive. The cell has therefore a preferred perimeter $P_0 = -2K_P/\gamma_P$. Using assumption (i) that the cells follow the deformation of the substrate during one cycle of stretching, we directly express the strain in the reference frame of the cells. Taking the long axis and the short axis of the cells, respectively, along the x and y directions (Fig. S1), we obtain $u_{xx}(t) = u(t)(\cos^2\theta - \nu\sin^2\theta)$, $u_{yy}(t) = u(t)(\sin^2\theta - \nu\cos^2\theta)$, and $u_{xy}(t) = u(t)(1+\nu)\cos\theta\sin\theta$. As a result, the cell area A_i varies as $A_i \to A_i(1 + u(t))(1 - \nu u(t))$ and it is independent of the orientation. By contrast, the amount of perimeter deformation depends on the orientation of the cells. To obtain the energy change per cell on stretching, we make the mean-field approximation that all shape properties of the cells except their angular orientation can be treated as identical. This is supported by the fact that we do not observe a significant correlation between the other shape parameters and the orientation angle in all experimental conditions. As a result, we write the energy stored per cell as

$$\delta E(\theta, t) = \frac{\gamma_P^2}{4K_p}(p(\theta, u(t)) - 1)^2. \tag{2}$$

where $p_i(\theta_i, u(t)) = P_i(\theta_i, u(t))/P_0$ is the ratio of the perimeter of ith cell with orientation θ_i under strain $u(t)$ with respect to the preferred perimeter value P_0 under no strain (see Appendix B for details).

As we observe in static stretching experiments (where $\delta E(\theta, t) = 0$) that the rotational diffusion is a much slower process than the stretching frequency, i.e., $D_b \ll \pi^2\omega$ where D_b is the BM-dependent rotational diffusion constant, and hence the mechanical energy gain can be averaged over one period of stretching τ_{str}. We express the time-averaged mean-field energy function for each cell in a form similar to the theory of Ref. [25] to compare the orientational behavior of the cells in a tissue with that of isolated cells. This is given by

$$\langle \delta E(\theta)\rangle_{\tau_{\text{str}}} = \frac{3}{16} K u_0^2((1+\nu)\cos^2\theta + B(1-\nu) - 1)^2, \tag{3}$$

where K is an effective stiffness, and B is the anisotropy parameter of the cells defined in Appendix B. The anisotropy parameter B is a combination of the various elastic moduli along with the principal strain directions of the cells, and $B \to \infty$ for isotropic cells, while $B \to 1$ in the limit of strong anisotropy. The stability analysis using the energy function Eq. (3) suggests that there exist two regimes for the preferred direction θ^* (the minimum of the energy function) depending on the values of B and the Poisson ratio of the substrate ν: $\theta^* = \theta_s^* = \arccos(\sqrt{(1 - B(1-\nu))/(1+\nu)})$ when $B < 1/(1-\nu)$ and $\theta^* = \pi/2$ when $B \geqslant 1/(1-\nu)$. We determine the value of the anisotropy parameter by mapping the geometrical parameters of the vertex model to the parameters of the elastic model. This yields

$$B \approx \frac{\alpha}{\alpha - 1} \tag{4a}$$

$$K \approx \left(\frac{\alpha - 1}{\alpha + 1}\right)^2 \frac{\gamma_p^2}{2K_p}, \tag{4b}$$

where α is the aspect ratio of the cells (see Appendix B). Note that K would vanish for isotropic cells $\alpha = 1$ for which

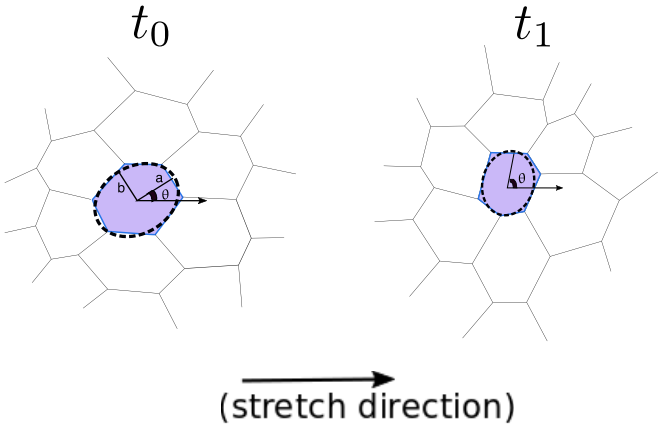

FIG. 3. Illustration of the rotational diffusion of the long axis of a cell. Even in the absence of mechanical strain, tissue cells exhibit shape fluctuations by rearranging their bonds and hence their shape parameters are different at times t_0 and t_1. The changes in the long axis orientation can appear as discrete jumps on the angle value; however, this can be neglected while averaging over all cells in the mean-field description. Accordingly, we model the fluctuations in orientation of the long axis as a rotational diffusion.

the energy function becomes independent of the orientation angle. For our experiments, using the mean value $\alpha = 1.8$, we estimate $B = 2.25$. Remarkably, the semiempirical observation by analyzing a digitally stretched image ($B^e \approx 2.29$, see Appendix B) validates this simple approach. For these parameters, we expect $\theta^* = \pi/2$ in accordance with our experimental results. This behavior is different from the result obtained in Ref. [25] with isolated fibroblasts that displays a preferred angular orientation $\theta^* = \theta_s^*$ whose value depends on both B and the effective Poisson ratio at the center of the chip. Accordingly, in that work, the anisotropy parameter is fitted with a value $B \approx 1.1$. Interestingly, Eq. (4) can also qualitatively reach this value for high aspect ratios that we would expect for fibroblasts even though we derived it using a vertex model. Similar studies on isolated cells having high aspect ratio $\alpha \gg 1$ and for which B approaches unity have also reported that the cells orient on average along the zero-strain direction [26,44,45] in agreement with our results. Thus the value of α seems to successfully determine the different regimes of orientational response. While this generality is remarkable, we should note that for large α values, our theory in Eq. (3) is no longer valid for confluent tissues as one needs to consider steric interactions leading to long-range correlations between cells displaying nematic order.

As a whole, the effective dynamics of each cell can be written in the Langevin form

$$\frac{d\theta}{dt} = -\frac{1}{\eta_b}\frac{\partial\langle\delta E(\theta)\rangle_{\tau_{\rm str}}}{\partial\theta} + \sqrt{2D_b}\xi(t), \tag{5}$$

where η_b is the BM-dependent friction coefficient and $\xi(t)$ is a zero mean unit variance Gaussian white noise. The effective diffusive behavior with rotational diffusion constant D_b originates from the binding rearrangements of the cells due to both intracellular processes and interactions with their surroundings (Fig. 3). These dynamics in principle entail an active noise spectrum which we simplified to explain the current experiments. Similar approaches have been used in modeling cell migration polarity [46–48]. These dynamical equations can be transformed into a Fokker-Planck equation for the probability distribution $\rho(\theta, t)$

$$\frac{\partial\rho(\theta,t)}{\partial t} = \frac{\partial}{\partial\theta}\left(\frac{1}{\eta_b}\frac{\partial\langle\delta E(\theta)\rangle_{\tau_{\rm str}}}{\partial\theta}\rho(\theta,t)\right) + D_b\frac{\partial^2}{\partial\theta^2}\rho(\theta,t). \tag{6}$$

We can deduce the angular distribution of the cells as a function of time from the Fokker-Planck equation. To probe the tendency of orientation, we define an order parameter

$$\bar{\phi}(t) = \langle\cos^2\theta\rangle_t, \tag{7}$$

where the bracket $\langle\rangle_t$ denotes an average performed over the distribution $\rho(\theta, t)$. For an ensemble with random orientations $\bar{\phi}(t) = 0.5$, whereas $\bar{\phi}(t) = 0$ or 1, respectively, for purely perpendicular and parallel orientations. Approximating the probability distribution $\rho(\theta, t)$ by a Gaussian function (see Appendix B 2), we obtain a simple form of the order parameter as a function of time

$$\bar{\phi}(t) = \bar{\phi}_{ss} + (0.5 - \bar{\phi}_{ss})e^{-t/\tau_{\rm rel}} \tag{8}$$

using the boundary conditions $\bar{\phi}(0) = 0.5$ and $\bar{\phi}_{ss} = \bar{\phi}(\infty)$ obtained from the experimental results. The relaxation time depends on both the stored elastic energy and the rotational diffusion constant and is given by

$$\tau_{\rm rel}^{-1} = D_b\left(4 + \frac{3\kappa_b u_0^2(1+\nu)^2}{32}\right), \tag{9}$$

where $\kappa_b = K/\eta_b D_b$. For small deformations, the steady-state value of the order parameter becomes

$$\bar{\phi}_{ss} \approx \tfrac{1}{2} + \tfrac{3}{128}(1-2B)\kappa_b(1-\nu^2)u_0^2. \tag{10}$$

As our analysis shows $B \geqslant 1$ [Eq.(4)] and since $\nu < 1$, the second term is negative. Note that for isotropic cells as $\alpha = 1$, $\kappa_b = 0$ since $K = 0$ from Eq. (4) leading to $\bar{\phi}_{ss} = 0.5$. On the other hand, increasing κ_b enhances the perpendicular orientation of cells as $\bar{\phi}_{ss}$ becomes lower than the random orientation value of 0.5.

In Fig. 4, we show the orientational response of the cells after 24 h of cyclic stretching [Figs. 4(b) and 4(c)] and the time evolution of the order parameter [Figs. 4(e) and 4(f)], together with the theoretical curve. During the reorientational dynamics, we observe a transition between a random distribution of orientations $\rho(\theta, t)$ and a Gaussian distribution centered around $\theta = \pi/2$ as the total stretching time t increases. The order-parameter $\bar{\phi}(t)$ decreases with the stretching time until it converges to its steady-state (long-time) value $\bar{\phi}_{\rm ss}$. For the theoretical analysis, we write the rotational diffusion constant as $D_b = T_b/\eta_b$ where T_b is a coating-dependent effective temperature that stems from the dynamical activity of the cells channeled to the rotational degree of freedom of the cell long axis. Thus T_b can alter the amplitude of the angular fluctuations independently from the rotational friction constant η_b. This allows us to evaluate the coating-dependent changes of the steady-state angular distributions and of the relaxation time separately. The steady-state probability distribution has a Boltzmann form $\rho^{\rm ss}(\theta) \sim e^{-\langle\delta E(\theta)\rangle_{\tau_{\rm str}}/T_b}$ which is a function of $\kappa_b = K/T_b$. Setting $B = 2.25$, we obtain the best-fit

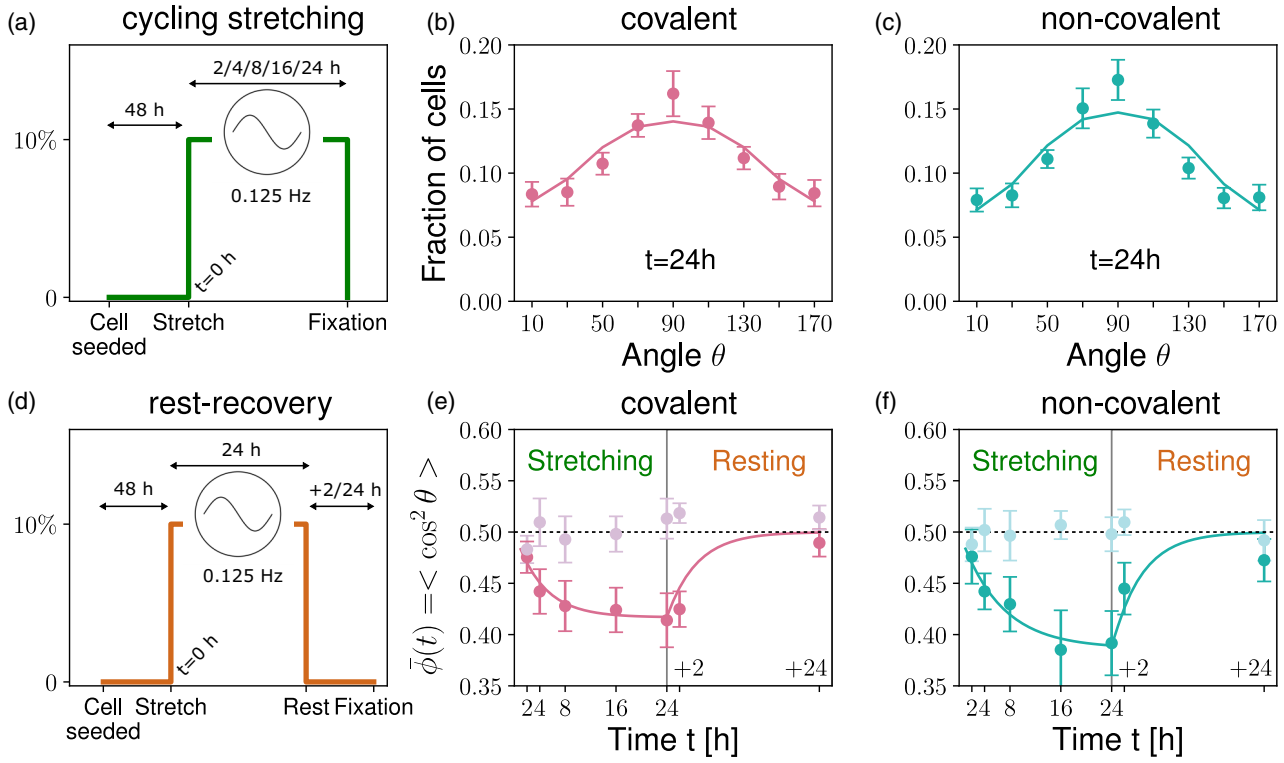

FIG. 4. Orientational response of cells. (a) Time frame of cyclic stretching. The cyclic stretching parameters are displayed in Fig. 2. We show the angular distribution of cells after a total period of 24 h cyclic stretching (b) for covalent coating and (c) for noncovalent coating conditions. Dots with error bars are experimental results and the solid line is the theoretical curve (see fit parameters in text). (d) Time frame of rest-recovery experiments. We show the time evolution of the order-parameter $\bar{\phi}(t)$ for different periods of cyclic stretching and rest-recovery periods (24 h stretching +2, +24 h rest). (e) for covalent coating and (f) for noncovalent coating conditions.

parameters as $\kappa_{\rm cov} = 128$, $D_{\rm cov} = 0.053\ {\rm h}^{-1}$ for covalently coated and $\kappa_{\text{non-cov}} = 178$, $D_{\text{non-cov}} = 0.036\ {\rm h}^{-1}$ for noncovalently coated laminin BM. Thus we observe that the rotational diffusion coefficient in the covalent condition is about 1.5 times higher than that of the noncovalent condition. We may understand this behavior by the facilitated diffusion of cells as the surface density of laminin is higher in covalently bound laminin coating [37]. On the other hand, κ_b has the inverse trend and the value $K/\eta_b = \kappa_b D_b$ does not depend on the coating condition. This intriguing conservation allows us to make the following speculation. In our previous analysis, K is obtained from an effective mapping which depends on the Poisson ratio of the substrate ν, the geometrical parameters of the cells, and the perimeter moduli K_P and γ_P (see Appendix B). Because we do not observe any difference in the morphologies of the cells in the covalent and noncovalent conditions, we can suppose that the values of K_P, γ_P and therefore of K are independent of the coating conditions, suggesting that the rotational friction constant η_b is also coating independent. Thus ruling out the sensitivity of these parameters on coating conditions leads to $T_{\rm cov} \approx 1.5 T_{\rm non-cov}$. This difference could be due to the fact that the energy transmission to the rotational degree of freedom of the cell long axis is depending on the surface density which differs in the two coating conditions. This could be due to the facilitated cell rearrangement events with enhanced adhesion; however, it requires further microscopic evidence to disentangle the effects of coating on both binding and unbinding events. Besides this hypothetical picture, we nevertheless conclude that the dynamical parameters remain within the same range for both coating conditions.

Finally, we performed rest-recovery experiments in which the confluent tissue first undergoes cyclic stretching during 24 h and then is left unstretched in position $u_0 = 0$ for an additional $t = 2$ or 24 h [4(e)]. The evolution of the order parameter is shown in Figs. 4(e) and 4(f) (gray regions), respectively, for covalent and noncovalent conditions. We observe a recovery to the isotropic state with uniform angle distribution showing that the angular response is reversible, in agreement with our theoretical description. We conclude that the dynamics are consistent with a rotational diffusion under an external mechanical stimulus. Thus in the absence of potential, i.e., $u_0 = 0$ in rest-recovery time line, the diffusive relaxation rate $\tau_{\rm rel}^{-1} = 4D_b$ approximately captures the experimental trend for both conditions.

D. The correlations are short ranged and decay exponentially

We also studied the range of the spatial correlations of orientation to determine whether local fluctuations can have long-range effects. For two cells at a normalized distance $\ell \equiv r/R$ where r is the actual distance and R is the mean neighboring distance between neighboring cells in the tissue, we calculate the correlation function of the order

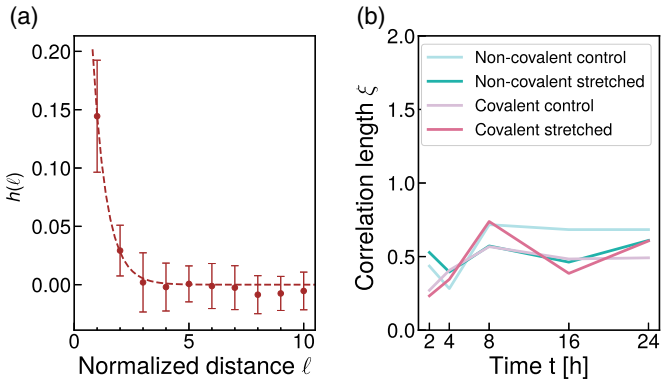

FIG. 5. Range of orientation correlations. (a) Correlation function $h(\ell)$ as a function of normalized distance ℓ in the covalent coating condition after $t = 24h$ of cyclic stretching. We observe that the correlations decay exponentially with a correlation length $\xi \lessapprox 1$ and are even shorter range than the mean neighboring distance between cells. In (b), we show that ξ is independent of coating condition and total time of stretching.

parameter

$$h(\ell, t) = \frac{\langle \phi(\ell)\phi(0)\rangle_t}{\bar{\phi}(t)^2} - 1. \tag{11}$$

Here the averaging is performed at a given time point over all cell pairs. We observe that the correlations in cell reorientation are not long range. In Fig. 5(a), we give an example of the calculated correlation function in covalent conditions under a total of $t = 24$ h cyclic stretching. Moreover, the correlation function has an exponential decay $h(\ell, t) \sim e^{-l/\xi}$ where the correlation length ξ appears independent of coating and stretching conditions [Fig. 5(b)]. In all cases, the correlation length is very short $\xi \lessapprox 1$, which justifies our mean-field approach where we treated the dynamics of each cell independently.

On the other hand, the exponential decay of the correlations indicates that our system is away from algebraic ordering which is ubiquitous in 2D systems with polar degrees of freedom where the correlations decay as a power law. In principle, the motility levels and the geometrical characteristics of Caco-2 cells can be the limiting factors. It would be interesting to see how these characteristics change in other cell types under cyclic stretching and whether a theory beyond the mean-field approach would be necessary.

III. CONCLUSIONS AND OUTLOOK

In this work, we have studied the reorganization of intestinal tissue under cyclic stretching mimicking *in vivo* peristalsis. Peristalsis aims at propelling the food through the gastrointestinal tract under the control of nerves, muscles, and pacemaker cells. Impairing this movement can lead to several pathologies such as chronic intestinal pseudo-obstruction [49]. To assess the effect of peristalsis on gut epithelium, we designed an original stretcher along with specific PDMS chips compatible with conventional cell culture conditions allowing the application of a controlled cyclic mechanical deformation to an intestinal epithelial monolayer. Thus we recapitulated the mechanical environment felt by epithelial cells in the intestine with a controlled stretching in terms of frequency, amplitude, duration and cyclic patterns. We have evaluated different laminin coating strategies (covalent and noncovalent) to understand their contribution to the signal mechanotransmission. Our results highlight a significant sensitivity to peristaltic-like stimuli of the angular orientation of the long axes of the cells with respect to the stretching axis with about 20% of the cells oriented with an angle ranging from 80 to 100°, whereas the other morphological parameters of the cells remain unchanged.

Earlier literature focused on the orientational response of isolated and highly contractile cells with high aspect ratio under cyclic stretching. The total yield and dynamics of cells are dependent on their elastic anisotropy, the stretching frequency, and the effective biaxiality ratio [25,44]. Here we have studied for the first time the orientational response of intestinal epithelium in details. In particular, peristaltic-like stimuli fall into the fast regime as it is faster than the topological rearrangement of cells. We show an equivalent approach from the vertex model which can be mapped to effective elastic theories. Thus we propose a unifying theoretical framework to study the orientational dynamics for different types of cells by relating their geometrical properties to elastic ones. We model the orientational dynamics in tissue cells as a viscoelastic process along the rotational axis with a characteristic autocorrelation time $\tau_{\text{rel}} \sim$ 5-7 h. The discrepancy between covalent and noncovalent conditions is small, while the latter has slower relaxation dynamics. Thus one can also argue the facilitated diffusion of cells on covalently coated laminin surface as there may be more available stable binding sites for cells [34], yet this would require microscopic examination of binding properties, which is beyond our scope in this paper. For our purposes, we conclude that the two conditions do not display a significant physiological difference.

Moreover, forces can also affect cell migration. Chaturvedi *et al.* have studied the effect of repetitive deformation on wound closure of Caco-2 monolayer, showing that cell motility can be either stimulated or inhibited depending on the nature of the adhesion molecules [4]. The effect of stretching on cell migration has also been studied for many other cell types, for example by Zhang *et al.* who showed that cyclic stretching promotes bone marrow stem cell migration while slightly inhibiting cell invasion [50]. A recent work has shown that stretching forces could also induce the alignment of fibronectin secreted by human prostatic fibroblasts as well as a persistent codirectionality of cancer cell migration when cocultured with stretched fibroblasts [51]. Taken together, these results suggest that stretching is prone to inducing a change in cell migration properties. How this change of cell orientation under cyclic stretching contributes to an increased cell migration remains to be understood. Indeed, recent work from Krndija *et al.* [1] has demonstrated that gut homeostasis relies on active migration of intestinal cells along the crypt to villus axis, opening fundamental questions about gut homeostasis [52]. Among those, how biochemical and mechanical cues contribute to the polarity of the cell sheet is still under investigation. At this stage extrapolation between *in vitro* and *in vivo* studies remains elusive as the pattern of stretching forces experienced *in vivo* by intestinal cells is way more

complex than the cyclic stretching applied here. Besides this and as mentioned earlier, *in vivo* intestinal cells are grown on a 3D scaffold and are subjected to different curvatures being in a different configuration when compared with the flat PDMS membrane used here for cell culture. This is why the microfabrication process has been designed so that a stretchable 3D scaffold can easily replace the flat PDMS substrate. In parallel, further technological developments to combine on-chip stretching and live high-resolution imaging are ongoing in order to study the cell response to stretching in time and space. Our work paves the way for further studies performed with primary cells stretched on a 3D deformable scaffold to decipher the role of the mechanical cues on intestinal cell migration in 3D.

ACKNOWLEDGMENTS

We acknowledge support from the Labex Cell(n)Scale (ANR-11-LABX-0038, ANR-10-IDEX-0001-02) and we also acknowledge DIM ELICIT for funding. This work has received the support of "Institut Pierre-Gilles de Gennes" (laboratoire d'excellence, "Investissements d'avenir" program ANR-10-IDEX-0001-02 PSL, ANR-10-LABX-31, ANR-10-EQPX-34, ANR project HOMEOGUT and Holifab (H2020-EU.2.1.2. H2020-NMBP-PILOTS-2017, Grant Agreement 760927).

L.G., E.I., J.-L.V., D.M.V., J.-F.J., and S.D. participated to the design research design; L.G. built the experimental platform; C.C. characterized the experimental platform; L.G. and M.B.-D. performed experiments; L.G. and E.I. participated in data analysis and interpretation; E.I. and J.-F.J. developed the theoretical models; and L.G., E.I., D.M.V., J.-F.J., and S.D. wrote the paper.

APPENDIX A: MATERIALS AND METHODS

1. Chip fabrication and coating

A brass mold was prepared by micromilling (Minitech). The PDMS ship was molded directly onto the brass mold prepared with PDMS (Sylgard 184, Dow Corning) with a prepolymer/curing agent at ratio 10:1 (w/w). The mold has been designed to fabricate chips with a central reservoir for cell culture medium compatible with long-term cell culture, a flat-bottom membrane compatible with cell stretching (thickness 1 mm), and connectors to be directly plugged into the chips on the stretcher. Another possible refinement of the device relies on the possibility to further micromill the central part of the mold to change at will the 3D structure of the bottom of the chip. To perfectly control the brass mold positioning and consequently the chip wall thickness, all parts of the molds were screwed and poured 7 ml of PDMS (1:10) and left to cure at 70°C for at least 3 h. After demolding, chips were sterilized in an ethanol bath (70%). Then we use two different coating protocols:

(i) *Noncovalent coating* requires the activation of the surface by a O_2 plasma treatment, then a solution of laminin (Natural Mouse, from Invitrogen 23017-015) at 0.02 mg/ml is incubated for 1 h at 37°C and washed three times with water. In this condition, the laminin coating mainly relies on electrostatic, hydrogen, and Van der Waals interactions.

(ii) *Covalent coating* requires the activation of the surface by a O_2 plasma treatment, then a solution of (3-aminopropyl) triethoxy-silane (APTES) at 0.5% (v/v) is incubated for 30 min and then rinsed three times with deionized water, and the chip is incubated for 30 min with a solution of cross-linker glutaraldehyde at 2% (v/v). Finally, the chip is rinsed overnight with deionized water, sterilized with ethanol, and incubated with laminin (0.02 mg/ml) for 1 h at 37°C.

2. Cell culture

Caco-2 cells are plated on the laminin-coated chips with a cell concentration of 200,000 cells/chip, allowed to adhere to the surface for 24 h, then medium is refreshed every 24 h. After 48 h of culture, cells reach confluency and three chips are placed on the stretcher and three are let free as control conditions; all were placed in a conventional cell culture incubator. For all experiments, the medium used was DMEM (1×) + GlutaMAX (ThermoFisher Scientific 31966 − 021) with 10% of fetal bovine serum (ThermoFisher scientific 26140079), 1% of antibiotico-antimycosique (ThermoFisher Scientific 15240062), and 1% of MEM nonessential amino acids solution (ThermoFisher Scientific 11140035) [53].

3. Staining protocol

We fix the cells using a solution of PFA/PBS at 4% (v/v) for 30 min at room temperature, then we rinse three times with PBS during 30 min and keep the chip in PBS overnight. We incubate the chips with Triton X-100/PBS at 0.5% (v/v) for 5 min at room temperature (500 μl of permeabilization solution per chip). We incubate the chips with the *blocking buffer* (0.2% of Triton X-100/2% BSA/3% normal goat serum) for 2 h at room temperature (500 μl blocking buffer per chip). We incubate the chips with primary antibodies in the *working buffer* (0.2% Triton X-100/0.1% BSA/0.3% normal goat serum) for 2 h at room temperature. The primary antibody ZO1 monoclonal (ThermoFisher scientific 33 − 9100) was used at 1/75th dilution and 300 μl of solution per chip were used. We wash three times with PBS for 30 min each at room temperature. We incubate the chips with secondary antibodies in the *working buffer* for 1 h at room temperature. The secondary antibody goat anti-mouse AlexaFluor Plus 647 (ThermoFisher scientific *A*32728) was used at 1/100th dilution and 300 μl of solution per chip were used. We wash four times with PBS for 30 min each at room temperature. We mount the samples using a mounting medium (ThermoFisher scientific *P*36931). Then we store the slides horizontally at 4°C until image acquisition.

4. Image acquisition and analysis

After staining, images from five different fields per chip were taken using a 10× objective on a confocal microscope (Leica inverted confocal microscope DMi8). All experiments were repeated twice. Therefore, 30 images were obtained for every experiment for the stretched and control conditions. The 10× objective induces a wide field of view (1163.64 m × 1163.64 m). The graphics in the main text represent the distribution or the mean value inside each image and the error bars are the standard deviation between those 30 images. These

measures were obtained using IMAGEJ software [54] and in particular the plugin Tissue Analyzer [55]. More precisely, images were segmented after calibration of the segmentation setting. Then segmentation settings were applied to all the extracted images, and parameters such circularity, aspect ration, etc were obtained using Tissue Analyzer plugin.

APPENDIX B: MODELING THE ORIENTATIONAL RESPONSE OF EPITHELIAL CELLS UNDER STRETCHING

We follow the assumptions stated in the main text. These suggest: (i) Cells deform together with the substrate and hence passively follow the stretch direction at short times ($t \sim \tau_{\rm str}$) where $\tau_{\rm str} = 2\pi/\omega$ is the period of stretching. (ii) At long time scales ($t \gg \tau_{\rm str}$), the long axis of cells undergoes a rotational diffusion. Thus the cells release this energy through a dissipative process in which they rearrange their shapes and boundaries. Under these assumptions, we need to calculate the mechanical energy stored by the cells due to deformation of the substrate. We first use a vertex model. Then we show a mapping to an effective continuum elastic model similar to that for isolated cells such as fibroblasts. We highlight the similarities and the differences between isolated cells and cells in a tissue.

1. Mechanical energy

a. Vertex model and mean energy injected per cell

We first investigate the cell deformations through the vertex model which is widely used for studying the dynamics of 2D confluent tissues. For a tissue containing N cells, the total mechanical energy is given by $E = E(\{\mathbf{r}_i\})$ [41,42],

$$E_{\rm tot} = \sum_{i=1}^{N} K_A (A_i - A_0)^2 + \gamma_P P_i + K_P P_i^2, \tag{B1}$$

where each cell is labeled by an index i while A_i and P_i are, respectively, the area and the perimeter of cell i. The energy related to changes in area is quadratic around an optimal cell area A_0 fixed by the interplay between cell volume incompressibility and the limiting resistance to height fluctuations. The second term proportional to the cell perimeter P_i is a line tension due to both cell-cell adhesion and cortical tension. We can separate these two contributions to the line tension as $\gamma_P = -\gamma_P^A + \gamma_P^T$: If $\gamma_P < 0$, then adhesion dominates and vice versa. The last term proportional to K_P is the elastic contribution due to actomyosin contractility and is quadratic in the perimeter of the cell P_i. Thus the cells have a preferred perimeter $P_0 = -\gamma_p/2K_p$ which we consider to be identical for each cell with the choice of homogeneous K_P and γ_P values. The ground-state configuration of the tissue is found by minimizing the total mechanical energy $E_{\rm tot}$. Here we focus on the change of total energy function due to the external mechanical strain applied on the substrate. We can express this perturbation for each cell as a function of the cell's long axis orientation angle. On stretching, the area of the cell A_i varies as $A_i \to A_i(1 + u(t))(1 - \nu u(t))$ and hence it is independent of the orientation. By contrast, the perimeter varies as a function of orientation angle and the change in total energy

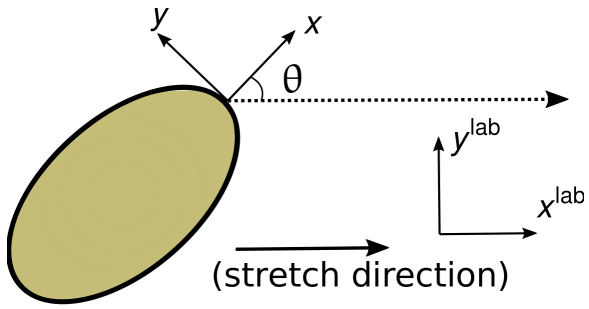

FIG. 6. Illustration of the coordinate axes. In our analysis, each cell is described by a best-fit ellipse with semi-major axis a (along x-direction), semi-minor axis b (along y-direction), and angle of orientation θ which is the angle between the semi-major axis and the stretching direction. $(x^{\rm lab}, y^{\rm lab})$ corresponds to lab frame, where the stretching occurs along $x^{\rm lab}$-direction. The cell's principal axes frame (x, y) can be obtained with by rotation of the lab frame by an angle θ which is defined so that x is the long-axis of the cell.

is given by

$$\delta E_{\rm tot}(t) = \sum_{i=1}^{N} K_p P_i^2 \big(p_i(\theta_i, u(t))^2 - 1\big) + \gamma_P P_i (p_i(\theta_i, u(t)) - 1) + \text{angle-indep. terms}, \tag{B2}$$

where $P_i(\theta_i, u(t))$ is the perimeter of ith cell with an orientation θ_i under strain $u(t)$, and $p_i(\theta_i, u(t)) = P_i(\theta_i, u(t))/P_i$ is its ratio in reference to the perimeter value P_i under no strain. Therefore the minimization of $\delta E_{\rm tot}(t)$ corresponds to a minimization of the change of the cell perimeter on stretching.

In order to obtain the mechanical energy injected per cell during stretching, we use a mean-field approach. Accordingly, we set $P_i = P_0 = -2\gamma_P/K_P$ and obtain the average energy per cell from Eq. (B2),

$$\delta E(\theta, t) = \frac{\gamma_P^2}{4K_p} (p(\theta, u(t)) - 1)^2. \tag{B3}$$

Thus $\delta E(\theta, t)$ is a function of the cell orientation angle and we drop the index i considering the dynamics of each cell identical yet dependent on θ.

b. Effective elastic theory

We next consider the cells as anisotropic elastic materials along the lines of the model introduced in Ref. [25] that we reformulate in a slightly different form using Cartesian coordinates. In continuum elasticity, the stored energy due to the deformation of an elastic material is given by [56]

$$\mathcal{H} = \tfrac{1}{2} \tilde{\lambda}_{ijkl} u_{ij} u_{kl}, \tag{B4}$$

where $\tilde{\lambda}_{ijkl}$ is the elastic modulus tensor; u_{ij}, u_{kl} is the strain or deformation tensor. The indices i, j, k, l denote the Cartesian components and we use the Einstein summation convention. We use the notation $(x^{\rm lab}, y^{\rm lab})$ for the coordinates in the laboratory reference frame and (x, y) for the coordinates in the reference frame of the cell as shown in Fig. 6. Using the symmetries for plane stress, we obtain the elastic strain energy of the cell that is integrated over the area of

the cell,

$$\mathcal{H}_{\text{cell}} = \tfrac{1}{2}\lambda_{xxxx}u_{xx}^2 + \tfrac{1}{2}\lambda_{yyyy}u_{yy}^2 + \lambda_{xxyy}u_{xx}u_{yy} + 2\lambda_{xyxy}u_{xy}^2, \tag{B5}$$

which involves four independent moduli associated to the anisotropic response of the cells, and $\lambda_{ijkl} = A_0\tilde{\lambda}_{ijkl}$ has units of energy. Stretching deforms each point on the substrate by a time varying strain along x^{lab} direction with frequency ω: $u_{xx}^{\text{lab}}(t) \equiv u(t) = \frac{1}{2}u_0(1-\cos\omega t)$. The resulting compression along the y^{lab} axis is $u_{yy}^{\text{lab}}(t) = -\nu u(t)$ where ν is the Poisson ratio of the substrate. More generally, if one controls the elastic strains along x^{lab} and y^{lab} independently, ν should be replaced by the measured magnitude of biaxiality strain ratio $u_{yy}^{\text{lab}}/u_{xx}^{\text{lab}}$ at the center of the chip. The elastic strains due to the stretching of the substrate can be transformed to the cell's reference frame as $u_{xx}(t) = u(t)(\cos^2\theta - \nu\sin^2\theta)$, $u_{yy}(t) = u(t)(\sin^2\theta - \nu\cos^2\theta)$ and $u_{xy}(t) = u(t)(1+\nu)\cos\theta\sin\theta$. Inserting these strains, we obtain the angle-dependent part of the elastic energy as

$$\mathcal{H}_{\text{cell}}(\theta,t) = \tfrac{1}{2}Ku^2(t)((1+\nu)\cos^2\theta + B(1-\nu) - 1)^2. \tag{B6}$$

Thus the stored elastic energy per cell depends on only two cell-related parameters. The anisotropy parameter B and the elastic coupling constant K are given by

$$B = \frac{\lambda_{xxxx} - (\lambda_{xxyy} + 2\lambda_{xyxy})}{\lambda_{xxxx} + \lambda_{yyyy} - 2(\lambda_{xxyy} + 2\lambda_{xyxy})} \tag{B7a}$$

$$K = B^{-1}(\lambda_{xxxx} - (\lambda_{xxyy} + 2\lambda_{xyxy})). \tag{B7b}$$

The anisotropy parameter B is dimensionless and the modulus K has units of energy. The energy function Eq. (B6) has the same form obtained in Ref. [25] for isolated cells (note that the definition of K is different).

c. Crossover between preferred orientations determined by elastic anisotropy

In the energy function given in Eq. (B6), B is the key parameter that determines the preferred direction for long axis orientation for cells. B itself is determined by the level of elastic anisotropy; weakly anisotropic cells reach $B \gg 1$ and the energy function becomes independent of the orientation angle, whereas strong anisotropy leads to $B \to 1$ which we will illustrate further below. The stability analysis of the elastic energy Eq. (B6) shows that there are two regimes for the preferred cell orientation (given by the minimum of the elastic energy),

$$\theta^* = \begin{cases} \theta_s^* = \arccos\left(\sqrt{\frac{1-B(1-\nu)}{1+\nu}}\right) & \text{for } B < 1/(1-\nu), \\ \pi/2 & \text{for } B \geqslant 1/(1-\nu). \end{cases} \tag{B8}$$

Thus when $B < 1/(1-\nu)$, the preferred angle θ_s^* depends on both the substrate (PDMS) Poisson ratio ν and the cell anisotropy parameter B. For strongly anisotropic cells, $B \to 1$ and hence θ_s^* approaches the zero-strain orientation, i.e., $\theta_s^* \to \arccos(\sqrt{\frac{\nu}{1+\nu}})$. Isolated fibroblast cells orient in mirror-image directions given by a value of θ^* that depends on both ν and B which allows to determine the value of B from experiments [25]. By contrast, for cells in a confluent tissue, the anisotropy is weaker and our results show that the cells tend to orient perpendicular to the stretch direction. Thus the observation of the preferred angle is not a determinant to deduce B except that we should expect $B \geqslant 1/(1-\nu)$. The rheology experiments on the tissue can be used to measure the elastic moduli λ_{ijkl} in order to obtain B and K, however, they would yield tissue level properties. On the other hand, we are interested in distinguishing the anisotropy at the cell level which is the main feature shaping the orientational response of cells. In the following, we estimate the anisotropy parameter B purely from the geometrical properties of tissue cells by using the vertex model.

d. Determination of the anisotropy parameter B from the vertex model

We can map the mean energy per cell obtained from the vertex model in Eq. (B3) to the form of energy function in Eq. (B6) and obtain the anisotropy parameter B. In order to do so, we need to estimate the fractional change in perimeter as a function of orientation angle θ and applied strain $u(t)$.

a. Simple ellipse assumption:. The simplest approach is to approximate each cell by an ellipse with short and long axes a and b, respectively. If we then approximate the perimeter by $P \approx \pi(a+b)$ and apply strains along the axes of the cell, we obtain $\delta E(\theta,t) = \mathcal{H}_{\text{cell}}(\theta,t)$ with parameters

$$B = \frac{\alpha}{\alpha - 1} \tag{B9a}$$

$$K = \left(\frac{\alpha-1}{\alpha+1}\right)^2 \frac{\gamma_p^2}{2K_p}, \tag{B9b}$$

where we define the aspect ratio $\alpha = a/b$. Our result remarkably agrees with isolated cell results so that $B \to 1$ for strong anisotropy as $\alpha \gg 1$, whereas K vanishes for isotropic systems $\alpha = 1$ and the energy function becomes independent of the orientation angle. For our experimental system, using the observation that the mean value of the aspect ratio $\alpha = 1.8$, we obtain $B = 2.25$.

b. Semiempirical approach:. We also measured the value of the anisotropy parameter B using empirical considerations. From our image analysis, we first obtain the perimeter values $P_i(\theta_i)$ and orientation angle θ_i for each cell. Then, we stretch the same image digitally with $u_{xx}^{\text{lab}} = u$, $u_{yy}^{\text{lab}} = -\nu u$ and perform an image analysis in order to obtain the stretched perimeter value $P_i(\theta_i, u)$ for each cell. Then we define $\delta p(\theta_i, u) = (P_i(\theta_i, u) - P_i)/P_i$ and perform a chi-square fitting to a function,

$$\delta p(\theta_i, u) = c_1\cos^2\theta_i + c_2 \tag{B10}$$

using $u = 0.1$ with fitting coefficients c_1 and c_2. Now, if we call the empirical anisotropy parameter B^e and use the quadratic form in Eq. (B6), we find the following relation

$$\frac{c_1}{c_2} = \frac{2(1+\nu)}{B^e(1-\nu-1/B^e)} \tag{B11}$$

from which we obtain $B^e \approx 2.29$.

2. Rotational dynamics

The configuration of the cells in the tissue constantly deviates from the ground state of the entire network due to active processes [57]. The system displays many alike preferred configurations. As illustrated in Fig. 3, we link this behavior including all the topological transitions (T1 and T2 transitions [58], and cell divisions) to the rotational diffusion of the long axis of cells. If we now define a BM-dependent rotational diffusion coefficient D_b and friction constant η_b, we obtain the Langevin dynamics

$$\frac{d\theta}{dt} = -\frac{1}{\eta_b}\frac{\delta E(\theta,t)}{\partial\theta} + \sqrt{2D_b}\xi(t), \tag{B12}$$

where $\xi(t)$ is a zero mean unit variance Gaussian white noise. From the Langevin equation, we derive a Fokker-Planck equation to study the time evolution in terms of the probability distribution function $\rho(\theta,t)$ of the orientations. From the Fokker-Planck equation, we study in detail the time evolution of the tissue in the two periods of motion: (i) Cells moving under periodic stretching and (ii) the resting period which follows the stretching period and which the cell orientation relaxes in the absence of stretch. Having estimated the elastic anisotropy $B = 2.25$, we are left with three fitting parameters $\{\eta_b, D_b, K\}$ to determinethe following:

(i) *Periodic stretching:* We observe that rotational diffusion is a much slower process than the stretching frequency, $D_b \ll \pi^2\omega$. This allows us to average over one period $\tau_{\rm str}$ the time varying strain $u^2(t)$. We thus replace $u^2(t)$ by its time average $\langle u^2(t)\rangle = \tau_{\rm str}^{-1}\int_0^{\tau_{\rm str}} u^2(t)dt = (3/8)u_0^2$ in Eq. (B6). As a result, we obtain the time evolution of the probability distribution of cell orientations $\rho(\theta,t)$ as

$$\frac{\partial\rho(\theta,t)}{\partial t} = -\frac{3K}{8\eta_b}u_0^2(1+\nu)\frac{\partial}{\partial\theta}\sin 2\theta((1+\nu)\cos^2\theta + B(1-\nu)-1)\rho(\theta,t) + D_b\frac{\partial^2}{\partial\theta^2}\rho(\theta,t). \tag{B13}$$

This Fokker-Planck equation can be solved numerically starting from a uniform distribution at $t = 0$, i.e., $\rho(\theta(0)) = 1/\pi$ with periodic boundary conditions such that $\rho(0,t) = \rho(\pi,t)$ and $\rho_\theta(0,t) = \rho_\theta(\pi,t)$ where $\rho_\theta = \partial\rho/\partial\theta$. We focus on the time evolution of the order-parameter $\bar\phi(t) = \langle\cos^2\theta\rangle_t$ where the average is taken over the probability distribution $\rho(\theta,t)$. As mentioned in the main text, the order parameter measures the average orientation of the cell ensemble in the tissue; $\bar\phi(t) = 0.5$ for random orientations, $\bar\phi(t) = 1$ for purely parallel orientations, and $\bar\phi(t) = 1$ for purely perpendicular orientations. It can be obtained using Eq. (B13) by multiplying both sides with $\cos^2\theta$ and integrating over the angle θ. This yields

$$\frac{d}{dt}\langle\cos^2\theta\rangle_t = -k_0 - k_1\langle\cos^2\theta\rangle_t - k_2\langle\cos^4\theta\rangle_t - k_3\langle\cos^6\theta\rangle_t, \tag{B14}$$

where k_0, k_1, k_2, k_3 are the following constants:

$$k_0 = -2D_b, \tag{B15a}$$

$$k_1 = 4D_b\big(1 + \tfrac{3}{8}\kappa u_0^2(1+\nu)(B(1-\nu)-1)\big), \tag{B15b}$$

$$k_2 = \tfrac{3}{2}D_b\kappa u_0^2(1+\nu)(2+\nu-B(1-\nu)), \tag{B15c}$$

$$k_3 = -\tfrac{3}{2}D_b\kappa u_0^2(1+\nu)^2, \tag{B15d}$$

where

$$\kappa_b = K/\eta_b D_b. \tag{B16}$$

Approximating $\rho(\theta,t)$ by a Gaussian distribution centered around $\pi/2$, we can express the averages of higher moments in terms of the ensemble average of the order parameter at time t as $\bar\phi(t) = \langle\phi\rangle_t$. To do so, we first express

$$\cos^{2m}\theta = \frac{1}{2^{2m-1}}\left[\frac{1}{2}\binom{2m}{m} + \sum_{k=0}^{m-1}\binom{2m}{k}\cos\left[2(m-k)\theta\right]\right], \tag{B17}$$

where $\binom{x}{y}$ denotes the binomial coefficients. Then we use the fact that $\langle\cos 2m\theta\rangle_t \sim (\langle\cos 2\theta\rangle_t)^{m^2}$ for a Gaussian distribution. As $\langle\cos 2\theta\rangle_t \ll 1$, we ignore higher-order contributions that have $m > 1$ and obtain

$$\bar\phi(t) = \frac{\langle\cos 2\theta\rangle_t + 1}{2}, \tag{B18}$$

$$\langle\cos^4\theta\rangle_t \approx \bar\phi(t) - \tfrac{1}{8}, \tag{B19}$$

$$\langle\cos^6\theta\rangle_t \approx \tfrac{15}{16}\bar\phi(t) - \tfrac{5}{32}. \tag{B20}$$

We may then rewrite Eq.(B14) as

$$d\bar\phi(t)/dt = -\tau_{\rm rel}^{-1}(\bar\phi_t - \bar\phi_{ss}), \tag{B21}$$

where $\bar\phi_{ss} = \tau_{\rm rel}(\frac{1}{8}k_2 - k_0 + \frac{5}{32}k_3)$ is the steady-state value of the order parameter and $\tau_{\rm rel}^{-1} = k_1 + k_2 + \frac{15}{16}k_3$ is the relaxation rate. Using Eq. (B15), we obtain

$$\tau_{\rm rel}^{-1} = D_b\big(4 + \tfrac{3}{32}\kappa_b u_0^2(1+\nu)^2\big), \tag{B22}$$

whereas the steady-state value of the order parameter for small deformations ($\kappa u_0^2 \ll 128/3$) becomes

$$\bar\phi_{ss} \approx \tfrac{1}{2} + \tfrac{3}{128}(1-2B)\kappa_b(1-\nu^2)u_0^2. \tag{B23}$$

The solution of the differential equation for the order parameter is

$$\bar\phi(t) = \bar\phi_{ss} + (0.5 - \bar\phi_{ss})e^{-t/\tau_{\rm rel}} \tag{B24}$$

using the boundary conditions $\bar\phi(0) = 0.5$ and $\bar\phi(\infty) = \bar\phi_{\rm ss}$. With this form, we can determine the effective relaxation time $\tau_{\rm rel}$ by direct fit of the experimental data.

(ii) *Resting:* During the resting period (t = 24–48 h in Fig. 2), the cell orientation relaxes in the absence of any external potential. Thus $\delta E = 0$ ($u_0 = 0$) and the initial distribution is $\rho(\theta, t = 24\ {\rm h}) = \rho_{ss}(\theta)$. This is a pure rotational diffusion process,

$$\frac{\partial\rho(\theta,t)}{\partial t} = D_b\frac{\partial^2}{\partial\theta^2}\rho(\theta,t). \tag{B25}$$

Then, by applying the same manipulations as above, we have the form Eq.(B14) with $k_2 = k_3 = 0$ and $k_1 = 4D_b$, whose solution reads

$$\bar\phi^{\rm rest}(t) = 0.5 + (\bar\phi_{ss} - 0.5)e^{-4D_b t}. \tag{B26}$$

At long times, we recover $\bar\phi_t^{\rm rest} = 0.5$, i.e., a random cell orientation. In Fig 2 (main text) we observe a good agreement of this dynamics with the experimental results.

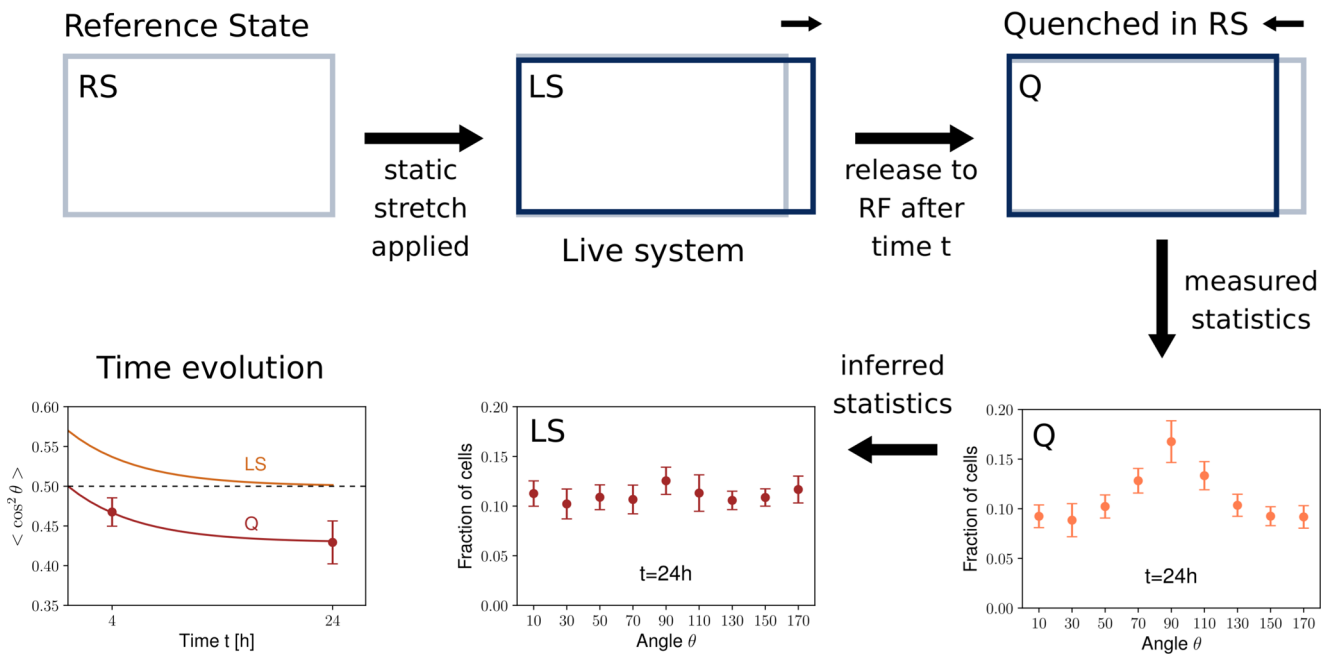

FIG. 7. Static stretching experiments. Cells are prepared on the regular chip which we name as the RS. Static stretch is applied while the cells are left to their dynamics for t hours (Live system: LS). After t hour, we release the applied stress and the cells are fixed right after. Thus the system is quenched in RS, which we refer as Q. The statistics are obtained in Q, and then by applying the (reverse) strain (purely geometrical), we obtain the inferred statistics. In the leftmost bottom graph, we show the time evolution of the order-parameter $\bar{\phi}(t) = \langle \cos^2\theta \rangle_t$ in both frames.

APPENDIX C: STATIC STRETCHING EXPERIMENTS

To probe the behavior of a Caco-2 cell monolayer in response to static stretching, we use the following procedure: First, the intestinal cells are seeded on the chips 48 h prior to the beginning of the stretching experiments. After 48 h of culture, the cells form a confluent monolayer that we refer to as the RS. We study here properties of the whole epithelium rather than the isolated cell's response to stretch. The chips are then subject to a static elongation in a pulled state (PS) for 4 to 24 h. For sustained elongation, the dynamics of epithelial cells take place during this stage PS. After each selected time period (4 h, 24 h), the stretcher is brought back to the RS and the cells are fixed. This final stage where the cells are fixed is referred to as the quenched state (Q) at which we perform the measurements.

These experimental results confirm our assumption on the existence of two different time regimes where the cells have different behaviors: (i) Cells remain attached and hence passively follow the stretch direction at short times. In principle, the stretcher device is moved from RS to PS and vice versa (PS to Q) in sufficiently short time that we observe only a passive behavior of the cells, i.e., the cells follow the substrate deformation. Thus by applying static strains u_{xx} and u_{yy} on each cell there is one-to-one mapping from Q to PS setup and vice versa. (ii) At long time scales, the long axis of the cells undergoes a rotational diffusion and recovers an isotropic distribution corresponding to random orientations. Once the cells start detaching, the effect of the mechanical stimulus is not maintained, and hence no mechanical energy is stored. In other words, the set point for zero strain becomes PS. Therefore $\delta E(\theta, t) = 0$ and using Eq. (B12), we have the Langevin form

$$\frac{d\theta}{dt} = \sqrt{2D_b}\xi(t), \tag{C1}$$

where D_b is the effective rotational diffusion constant of a cell in the confluent tissue and $\xi(t)$ is a zero mean unit variance Gaussian white noise.

Using the first assumption, we expect cells to orient parallel to the stretching axis at initial times, while in the absence of mechanical energy, they reorient in random directions at long times in LS following Eq. (C1). This is shown in detail in Fig. 7 in terms of the fraction of cells as a function of orientation angle θ. As shown in Fig. 7, the initial stretching leads to parallel orientation $\bar{\phi}^{\rm PS}(0) > 0.5$, while the orientational dynamics which is on the order of hours follow:

$$\bar{\phi}^{\rm PS}(t) = 0.5 + 0.07e^{-4D_b t}, \tag{C2}$$

where D_b is the effective rotational diffusion constant.

[1] D. Krndija, F. El Marjou, B. Guirao, S. Richon, O. Leroy, Y. Bellaiche, E. Hannezo, and D. M. Vignjevic, Active cell migration is critical for steady-state epithelial turnover in the gut, Science **365**, 705 (2019).

[2] C. P. Gayer and M. D. Basson, The effects of mechanical forces on intestinal physiology and pathology, Cell. Signalling **21**, 1237 (2009).

[3] H. J. Kim, H. Li, J. J. Collins, and D. E. Ingber, Contributions of microbiome and mechanical deformation to intestinal bacterial overgrowth and inflammation in a human gut-on-a-chip, Proc. Natl. Acad. Sci. USA **113**, E7 (2016).

[4] L. S. Chaturvedi, S. A. Saad, N. Bakshi, H. M. Marsh, and M. D. Basson, Strain matrix-dependently dissociates gut epithelial spreading and motility, J. Surg. Res. **156**, 217 (2009).

[5] D. Pinheiro and Y. Bellaïche, Mechanical force-driven adherens junction remodeling and epithelial dynamics, Dev. Cell **47**, 3 (2018).

[6] T. R. Huycke, B. M. Miller, H. K. Gill, N. L. Nerurkar, D. Sprinzak, L. Mahadevan, and C. J. Tabin, Genetic and mechanical regulation of intestinal smooth muscle development, Cell **179**, 90 (2019).

[7] K. M. Sanders, S. D. Koh, S. Ro, and S. M. Ward, Regulation of gastrointestinal motility–insights from smooth muscle biology, Nat. Rev. Gastroenterol. Hepatol. **9**, 633 (2012).

[8] A. Fatehullah, S. H. Tan, and N. Barker, Organoids as an in vitro model of human development and disease, Nat. Cell Biol. **18**, 246 (2016).

[9] T. Sato, R. G. Vries, H. J. Snippert, M. Van De Wetering, N. Barker, D. E. Stange, J. H. Van Es, A. Abo, P. Kujala, P. J. Peters *et al.*, Single lgr5 stem cells build crypt-villus structures in vitro without a mesenchymal niche, Nature (London) **459**, 262 (2009).

[10] M. Verhulsel, M. Vignes, S. Descroix, L. Malaquin, D. M. Vignjevic, and J.-L. Viovy, A review of microfabrication and hydrogel engineering for micro-organs on chips, Biomaterials **35**, 1816 (2014).

[11] S. N. Bhatia and D. E. Ingber, Microfluidic organs-on-chips, Nat. Biotechnol. **32**, 760 (2014).

[12] M. Nikolaev, O. Mitrofanova, N. Broguiere, S. Geraldo, D. Dutta, Y. Tabata, B. Elci, N. Brandenberg, I. Kolotuev, N. Gjorevski, H. Clevers, and M. P. Lutolf, Homeostatic mini-intestines through scaffold-guided organoid morphogenesis, Nature (London) **585**, 574 (2020).

[13] C. M. Costello, M. B. Phillipsen, L. M. Hartmanis, M. A. Kwasnica, V. Chen, D. Hackam, M. W. Chang, W. E. Bentley, and J. C. March, Microscale Bioreactors for in situ characterization of GI epithelial cell physiology, Sci. Rep. **7**, 12515 (2017).

[14] J. Creff, R. Courson, T. Mangeat, J. Foncy, S. Souleille, C. Thibault, A. Besson, and L. Malaquin, Fabrication of 3d scaffolds reproducing intestinal epithelium topography by high-resolution 3d stereolithography, Biomaterials **221**, 119404 (2019).

[15] J. Salomon, C. Gaston, J. Magescas, B. Duvauchelle, D. Canioni, L. Sengmanivong, A. Mayeux, G. Michaux, F. Campeotto, J. Lemale *et al.*, Contractile forces at tricellular contacts modulate epithelial organization and monolayer integrity, Nat. Commun. **8**, 13998 (2017).

[16] Y. Wang, D. B. Gunasekara, M. I. Reed, M. DiSalvo, S. J. Bultman, C. E. Sims, S. T. Magness, and N. L. Allbritton, A microengineered collagen scaffold for generating a polarized crypt-villus architecture of human small intestinal epithelium, Biomaterials **128**, 44 (2017).

[17] M. Verhulsel, A. Simon, M. Bernheim-Dennery, V. R. Gannavarapu, L. Gérémie, D. Ferraro, D. Krndija, L. Talini, J.-L. Viovy, D. M. Vignjevic *et al.*, Developing an advanced gut on chip model enabling the study of epithelial cell/fibroblast interactions, Lab Chip **21**, 365 (2021).

[18] S. A. Gudipaty, J. Lindblom, P. D. Loftus, M. J. Redd, K. Edes, C. F. Davey, V. Krishnegowda, and J. Rosenblatt, Mechanical stretch triggers rapid epithelial cell division through Piezo1, Nature (London) **543**, 118 (2017).

[19] L. S. Chaturvedi, H. M. Marsh, and M. D. Basson, Role of RhoA and its effectors ROCK and mDia1 in the modulation of deformation-induced FAK, ERK, p38, and MLC motogenic signals in human Caco-2 intestinal epithelial cells, A. J. Physiol. Cell Physiol. **301**, C1224 (2011).

[20] G. Samak, R. Gangwar, L. M. Crosby, L. P. Desai, K. Wilhelm, C. M. Waters, and R. Rao, Cyclic stretch disrupts apical junctional complexes in Caco-2 cell monolayers by a JNK-2-, c-Src-, and MLCK-dependent mechanism, Am. J. Physiol. Gastrointest. Liver Physiol. **306**, G947 (2014).

[21] H. J. Kim and D. E. Ingber, Gut-on-a-Chip microenvironment induces human intestinal cells to undergo villus differentiation, Integr. Biol. **5**, 1130 (2013).

[22] A. Grassart, V. Malardé, S. Gobaa, A. Sartori-Rupp, J. Kerns, K. Karalis, B. Marteyn, P. Sansonetti, and N. Sauvonnet, Bioengineered human organ-on-chip reveals intestinal microenvironment and mechanical forces impacting shigella infection, Cell Host Microbe **26**, 435 (2019).

[23] H. J. Kim, D. Huh, G. Hamilton, and D. E. Ingber, Human gut-on-a-chip inhabited by microbial flora that experiences intestinal peristalsis-like motions and flow, Lab Chip **12**, 2165 (2012).

[24] M. Kasendra, A. Tovaglieri, A. Sontheimer-Phelps, S. Jalili-Firoozinezhad, A. Bein, A. Chalkiadaki, W. Scholl, C. Zhang, H. Rickner, C. A. Richmond, H. Li, D. T. Breault, and D. E. Ingber, Development of a primary human Small intestine-on-a-chip using biopsy-derived organoids, Sci. Rep. **8**, 2871 (2018).

[25] A. Livne, E. Bouchbinder, and B. Geiger, Cell reorientation under cyclic stretching, Nat. Commun. **5**, 3938 (2014).

[26] R. De, A. Zemel, and S. A. Safran, Dynamics of cell orientation, Nat. Phys. **3**, 655 (2007).

[27] R. De and S. A. Safran, Dynamical theory of active cellular response to external stress, Phys. Rev. E **78**, 031923 (2008).

[28] S.A. Safran and and R. De, Nonlinear dynamics of cell orientation, Phys. Rev. E **80**, 060901 (2009).

[29] D. Huh, B. D. Matthews, A. Mammoto, M. Montoya-Zavala, H. Y. Hsin, and D. E. Ingber, Reconstituting organ-level lung functions on a chip, Science **328**, 1662 (2010).

[30] A. Jain, R. Barrile, A. D. van der Meer, A. Mammoto, T. Mammoto, K. De Ceunynck, O. Aisiku, M. A. Otieno, C. S. Louden, G. A. Hamilton *et al.*, Primary human lung alveolus-on-a-chip model of intravascular thrombosis for assessment of therapeutics, Clin. Pharmacol. Ther. **103**, 332 (2018).

[31] L. Wang, B. Sun, K. S. Ziemer, G. A. Barabino, and R. L. Carrier, Chemical and physical modifications to poly (dimethylsiloxane) surfaces affect adhesion of caco-2 cells, J. Biomed. Mater. Res. **93A**, 1260 (2010).

[32] I. C. Teller and J. F. Beaulieu, Interactions between laminin and epithelial cells in intestinal health and disease, Expert Rev. Mol. Med. **3**, 1 (2001).

[33] W. Li, A. Duzgun, B. E. Sumpio, and M. D. Basson, Integrin and fak-mediated mapk activation is required for cyclic strain

mitogenic effects in caco-2 cells, Am. J. Physiol. Gastrointest. Liver Physiol. **280**, G75 (2001).

[34] P.-J. Wipff, H. Majd, C. Acharya, L. Buscemi, J.-J. Meister, and B. Hinz, The covalent attachment of adhesion molecules to silicone membranes for cell stretching applications, Biomaterials **30**, 1781 (2009).

[35] C. Pereira, F. Araújo, C. C. Barrias, P. L. Granja, and B. Sarmento, Dissecting stromal-epithelial interactions in a 3D invitro cellularized intestinal model for permeability studies, Biomaterials **56**, 36 (2015).

[36] D. Louvard, M. Kedinger, and H. Hauri, The differentiating intestinal epithelial cell: establishment and maintenance of functions through interactions between cellular structures, Annu. Rev. Cell Biol. **8**, 157 (1992).

[37] A. J. Ribeiro, K. Zaleta-Rivera, E. A. Ashley, and B. L. Pruitt, Stable, covalent attachment of laminin to microposts improves the contractility of mouse neonatal cardiomyocytes, ACS Appl. Mater. Interfaces **6**, 15516 (2014).

[38] T. Yamashita, P. Kollmannsberger, K. Mawatari, T. Kitamori, and V. Vogel, Cell sheet mechanics: How geometrical constraints induce the detachment of cell sheets from concave surfaces, Acta Biomater. **45**, 85 (2016).

[39] T. P. Wyatt, A. R. Harris, M. Lam, Q. Cheng, J. Bellis, A. Dimitracopoulos, A. J. Kabla, G. T. Charras, and B. Baum, Emergence of homeostatic epithelial packing and stress dissipation through divisions oriented along the long cell axis, Proc. Natl. Acad. Sci. USA **112**, 5726 (2015).

[40] K. C. Hart, J. Tan, K. A. Siemers, J. Y. Sim, B. L. Pruitt, W. J. Nelson, and M. Gloerich, E-cadherin and lgn align epithelial cell divisions with tissue tension independently of cell shape, Proc. Natl. Acad. Sci. USA **114**, E5845 (2017).

[41] L. Hufnagel, A. A. Teleman, H. Rouault, S. M. Cohen, and B. I. Shraiman, On the mechanism of wing size determination in fly development, Proc. Natl. Acad. Sci. USA **104**, 3835 (2007).

[42] R. Farhadifar, J.-C. Röper, B. Aigouy, S. Eaton, and F. Jülicher, The influence of cell mechanics, cell-cell interactions, and proliferation on epithelial packing, Curr. Biol. **17**, 2095 (2007).

[43] D. Bi, J. Lopez, J. M. Schwarz, and M. L. Manning, A density-independent rigidity transition in biological tissues, Nat. Phys. **11**, 1074 (2015).

[44] J. H.-C. Wang, Substrate deformation determines actin cytoskeleton reorganization: A mathematical modeling and experimental study, J. Theor. Biol. **202**, 33 (2000).

[45] U. Faust, N. Hampe, W. Rubner, N. Kirchgessner, S. Safran, B. Hoffmann, and R. Merkel, Cyclic stress at mhz frequencies aligns fibroblasts in direction of zero strain, PLoS One **6**, e28963 (2011).

[46] D. Bi, X. Yang, M. C. Marchetti, and M. L. Manning, Motility-Driven Glass and Jamming Transitions in Biological Tissues, Phys. Rev. X **6**, 021011 (2016).

[47] D. L. Barton, S. Henkes, C. J. Weijer, and R. Sknepnek, Active vertex model for cell-resolution description of epithelial tissue mechanics, PLoS Comput. Biol. **13**, e1005569 (2017).

[48] M. Czajkowski, D. M. Sussman, M. C. Marchetti, and M. L. Manning, Glassy dynamics in models of confluent tissue with mitosis and apoptosis, Soft Matter **15**, 9133 (2019).

[49] K. S. Patel and A. Thavamani, *Physiology, Peristalsis* (StatPearls Publishing, Treasure Island, FL, 2021).

[50] B. Zhang, Q. Luo, Z. Chen, J. Sun, B. Xu, Y. Ju, and G. Song, Cyclic mechanical stretching promotes migration but inhibits invasion of rat bone marrow stromal cells, Stem Cell Res. **14**, 155 (2015).

[51] M. Ao, B. M. Brewer, L. Yang, O. E. F. Coronel, S. W. Hayward, D. J. Webb, and D. Li, Stretching fibroblasts remodels fibronectin and alters cancer cell migration, Sci. Rep. **5**, 8334 (2015).

[52] A. Kopf and M. Sixt, Gut homeostasis: Active migration of intestinal epithelial cells in tissue renewal, Curr. Biol. **29**, R1091 (2019).

[53] M. Natoli, B. D. Leoni, I. D'Agnano, F. Zucco, and A. Felsani, Good Caco-2 cell culture practices., Toxicol in Vitro **26**, 1243 (2012).

[54] J. Schindelin, I. Arganda-Carreras, E. Frise, V. Kaynig, M. Longair, T. Pietzsch, S. Preibisch, C. Rueden, S. Saalfeld, B. Schmid, J. Y. Tinevez, D. J. White, V. Hartenstein, K. Eliceiri, P. Tomancak, and A. Cardona, Fiji: An open-source platform for biological-image analysis, Nat. Methods **9**, 676 (2012).

[55] B. Aigouy, D. Umetsu, and S. Eaton, Segmentation and quantitative analysis of epithelial tissues, *Drosophila: Methods and Protocols*, edited by C. Dahmann (Springer, New York, 2016), pp. 227–239.

[56] L. D. Landau and E. M. Lifshitz, *Theory of Elasticity* (Mir, Moscow, 1990)

[57] D. B. Staple, R. Farhadifar, J.-C. Röper, B. Aigouy, S. Eaton, and F. Jülicher, Mechanics and remodelling of cell packings in epithelia, Eur. Phys. J. E **33**, 117 (2010).

[58] D. Weaire and N. Rivier, Soap, cells and statistics–random patterns in two dimensions, Contemp. Phys. **25**, 59 (1984).